Dear Author,

Please, note that changes made to the HTML content will be added to the article before publication, but are not reflected in this PDF.

Note also that this file should not be used for submitting corrections.

Computers and Geotechnics xxx (2016) xxx–xxx

Contents lists available at ScienceDirect

Computers and Geotechnics

journal homepage: www.elsevier.com/locate/compgeo

Research Paper

Comparison of Press-Replace Method and Material Point Method for analysis of jacked piles

Faraz S. Tehrani [a,*,1], Phuong Nguyen [b], Ronald B.J. Brinkgreve [c], A. Frits van Tol [b]

[a] Deltares, The Netherlands
[b] Faculty of Civil Engineering and Geosciences, Delft University of Technology, Deltares, Delft, The Netherlands
[c] Faculty of Civil Engineering and Geosciences, Delft University of Technology and Manager Research & Projects, PLAXIS BV, Delft, The Netherlands

ARTICLE INFO

Article history:
Received 30 May 2015
Received in revised form 27 April 2016
Accepted 28 April 2016
Available online xxxx

Keywords:
Jacked piles
Sand
Numerical analysis
Press-Replace method
Material Point Method

ABSTRACT

In this study, installation of jacked piles in sand is simulated using Press-Replace Method (PRM) and Material Point Method (MPM) and the results are compared together. This comparison is important because a realistic and yet efficient simulation of installation of jacked piles is an appealing step towards the design and analysis of this type of displacement piles. It is shown that PRM as a method that is founded on small-strain finite element method can produce pile and soil responses that are in a promising agreement with those of MPM which is a finite-deformation analysis method.

1. introduction

Pile installation using dynamic driving methods is associated with undesirable environmental effects such as noise, vibration and pollution. Therefore, pile jacking (pressing) has become attractive due to the environmental advantages that it has over conventional driving methods [1]. In addition to the environmental advantages, it is possible to estimate the ultimate load capacity of jacked piles during pile installation based on the measured jacking load [2]. Jacked piles, in their initial application, were mainly used to underpin existing foundations to increase their capacity and decrease their settlement [3]. Nowadays, there is an increasing trend in using jacked piles as foundations of new structures, in particular, in urban environment where minimizing the noise and vibration due to construction activities is desirable. Due to the tendency in using jacked piles, many researchers have studied jacked piles using experimental [2,4–10] and computational methods [1,11–13]. Furthermore, the simulation of jacked pile installation is a necessary and beneficial step towards simulating the installation of driven piles.

Realistic simulation of the installation process is a key step in analyzing the behavior of jacked piles. In the past years, number of researchers have focused on simulating the whole installation process using large-deformation numerical analysis methods such as Arbitrary Eulerian–Lagrangian (AEL) method [14,15] and its derivation, namely, Coupled Eulerian–Lagrangian (CEL) method [16,17], adaptive remeshing technique [11], and most recently Material Point Method (MPM) [18,19]. Besides finite-deformation analysis methods, a simpler method entitled Press-Replace Method (PRM) has been successfully used for simulation of jacked pile installation using small-deformation theory [20,21].

MPM has recently gained attentions in simulating large-deformation boundary and initial value problems in geotechnical engineering. Despite its promising performance, MPM is computationally expensive and relatively complicated which decrease its attraction for practice engineers who look for practical and straight-forward methods in a daily engineering practice. PRM, on the other hand, is a simple method that is based on small-deformation theory, which has been used solely for simulation of penetration problems such as pile jacking and cone penetration. The simplicity of PRM enables an engineer to model the installation process of jacked piles as a staged construction process by any finite element code. The purpose of this study is to compare PRM and MPM for numerical simulation of jacked piles during installation and operation. Such a comparison shows if the PRM can be relied upon for the analysis of jacked piles. It also reveals

* Corresponding author.
E-mail addresses: faraz.tehrani@deltares.nl (F.S. Tehrani), phuong.nguyen@deltares.nl (P. Nguyen), r.brinkgreve@plaxis.nl (R.B.J. Brinkgreve), a.f.vantol@tudelft.nl (A.F. van Tol).
[1] Formerly at Faculty of Civil Engineering and Geosciences, Delft University of Technology, The Netherlands.

http://dx.doi.org/10.1016/j.compgeo.2016.04.017
0266-352X/

Nomenclature

α	hypoplasticity parameter that determines the dependency of peak friction angle with respect to the relative density
β	hypoplasticity parameter that determines the dependency of soil stiffness with respect to the relative density
B	pile diameter
B_R	intergranular strain parameter of the hypoplastic model
C_c	coefficient of curvature
C_u	coefficient of uniformity
D_{50}	mean particle diameter
D_R	relative density
δ_c	critical-state interface friction angle
δ	interface friction angle
e	void ratio
e_{max}	maximum void ratio
e_{min}	minimum void ratio
e_{d0}	minimum reference void ratio in the hypoplastic model
e_{c0}	reference void ratio at the critical state in the hypoplastic model
e_{i0}	maximum reference void ratio in the hypoplastic model
E_p	Young's modulus of the pile material
$E_{oed,i}$	interface oedometric stiffness
ϕ	soil friction angle
ϕ_c	critical-state friction angle
ϕ_p	peak friction angle
G_s	specific gravity
G	soil shear modulus
G_i	interface shear stiffness
γ_d	soil dry unit weight
h_s	granular hardness, determines the inclination of the void ratio limits in the hypoplastic model
K_0	coefficient of lateral earth pressure at rest
L	pile length
m_R	intergranular strain parameter of the hypoplastic model
m_T	intergranular strain parameter of the hypoplastic model
n	hypoplasticity parameter that determines the curvature of the void ratio limits
Q_{sL}	limit shaft capacity
r	radial distance from the pile center
R_i	interface reduction factor
R_{max}	intergranular strain parameter of the hypoplastic model
σ_{rr}	radial stress
σ_{zz}	vertical stress
σ_{rz}	shear stress
t_s	thickness of soil slices in the PRM analyses
u_r	radial displacement
u_z	vertical displacement
v	soil Poisson's ratio
v_i	interface Poisson's ratio
w	pile head settlement
χ	intergranular strain parameter of the hypoplastic model
ψ	soil dilatancy angle
z	depth

the differences that exist between PRM and a more sophisticated method of pile installation simulation, namely MPM. For simplicity, this paper only focuses on the single-stroke jacking as an initial step in simulating the multi-stroke jacking of piles.

2. Analysis methods

2.1. Material Point Method

The Material Point Method (MPM) can be viewed as an extension of the Particle-In-Cell method (PIC) and was initially applied to fluid dynamic problem by Harlow [22]. Later on, Brackbill and his co-workers [23] developed the so-called fluid-implicit particle (FLIP) method, that is a PIC formulation, in which the particles carry all physical properties of the continuum. FLIP uses adaptive meshing which is able to model complex geometries and achieves better accuracy than does PIC. In 1994, the FLIP method was extended to adapt into solid mechanics by Sulsky et al. [24]. In the extended method, the weak formulation and the discrete equation are consistent with the finite element method (FEM). Furthermore, the constitutive equation is applied at each single particle, which allows the method to handle the history-dependent mate-

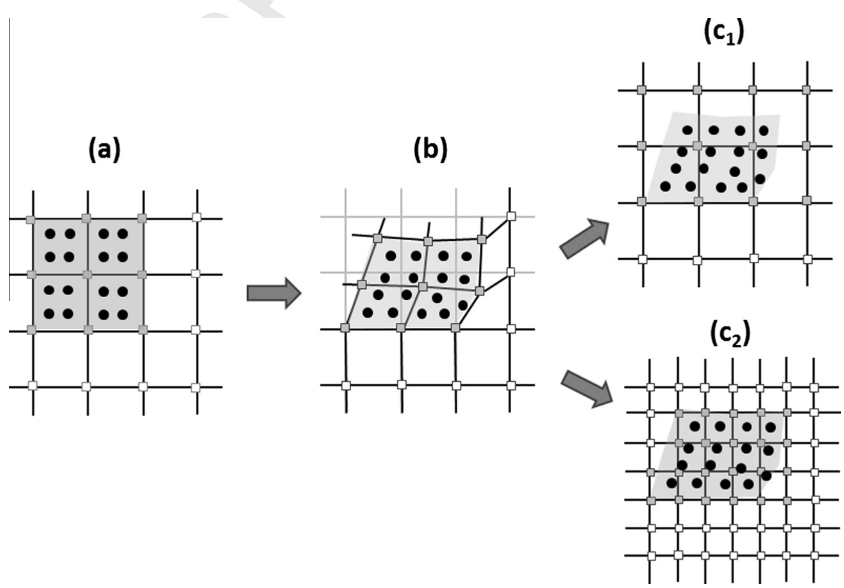

Fig. 1. The MPM solution algorithm: (a) initialization step, (b) incremental deformation (Lagrangian step) and (c_1) resetting the mesh or (c_2) redefining a new mesh (convective step).

Please cite this article in press as: Tehrani FS et al. Comparison of Press-Replace Method and Material Point Method for analysis of jacked piles. Comput Geotech (2016), http://dx.doi.org/10.1016/j.compgeo.2016.04.017

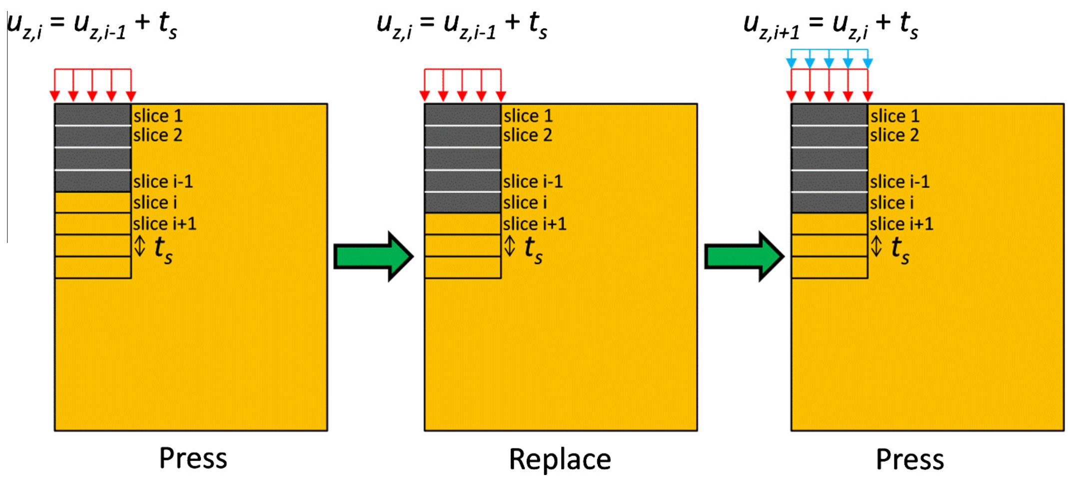

Fig. 2. Press-Replace technique.

rial behavior. In 1996, Sulsky and Schreyer [25] named the method as "material point method" and presented its axisymmetric formulation. Bardenhagen and Brackbil [26] used MPM to model the stress bridging and localization in granular materials under quasi static and dynamic loads. In 1999, Więckowski and his co-workers [27] applied the method to simulate the problem of silo discharge, which showed the potential of MPM for simulating flow of granular material. Sulsky [28] investigated the macroscopic stress–strain response of dry granular material under compression using MPM and showed that MPM is able to reproduce the experimental observations of stiffening of the granular material. In 2004, Bardenhagen and Kober [29] generalized the MPM algorithm by implementing the Petrov–Galerkin discretization scheme. They used the shape functions together with particle characteristic functions in the variational formulation. Different combinations of the shape functions and particle characteristic functions resulted in a family of methods labeled in [29] as the generalized interpolation material point (GIMP) methods. The main motivation to investigate GIMP was to eliminate the numerical noise associated with MPM when particles cross element boundary. Bardenhagen and Kober [29] showed in one-dimensional examples that GIMP is capable of eliminating the noise in stresses observed in an MPM solution. However, the use of Petrov–Galerkin discretization scheme deviates the method more towards meshless methods [29]. To date, several MPM simulation have been carried out to model large deformation problems in geotechnical engineering, including the pile installation problems [30–35].

The material point method can be regarded as an extension of a finite element procedure. It uses two types of space discretization: first, the computational mesh and second the collection of material points which move through an Eulerian fixed mesh. The material points carry all physical properties of the continuum such as position, mass, momentum, material parameters, strains, stresses, constitutive properties as well as external loads, whereas the Eulerian mesh and its Gauss points carry no permanent information. The advantage of MPM is that the state variables are traced automatically by the material points independent of the computational mesh. Therefore, MPM is well suited for modeling problems with large deformations. The governing equation of MPM is identical to the explicit formulation of FEM given by:

$$\mathbf{M}\ddot{\mathbf{u}} = \mathbf{F}^{ext} - \mathbf{F}^{int} \tag{1}$$

where $\mathbf{M}$ is the lumped mass matrix, $\ddot{\mathbf{u}}$ is the vector of nodal acceleration, and $\mathbf{F}^{ext}$ and $\mathbf{F}^{int}$ are the vectors of external and internal nodal forces, respectively.

Table 1
Basic properties of Baskarp sand [37].

SiO_2	D_{50} (mm)	C_c	C_u	G_s	e_{max}	e_{min}	ϕ_c (°)
⩾90%	0.14	0.90	1.33	2.645	1.018	0.542	30

Table 2
Hypoplastic soil model parameters for Baskarp sand [37].

ϕ_c (°)	h_s (MPa)	n	e_{d0}	e_{c0}	e_{i0}	α	β
30	4000	0.42	0.548	0.929	1.08	0.12	0.96

Note: $e_{d0} = e_{min}$ and $e_{i0} = e_{max}$.

Table 3
Small-strain stiffness hypoplasticity parameters for Baskarp sand [37].

m_R	m_T	R_{max}	B_R	χ
5	2	0.0001	1	1

The MPM solution algorithm can be divided into three steps: (a) the initialization step, (b) the Lagrangian step and (c) the convective step. These steps are shown in Fig. 1.

In the initialization step, all the information carried by the material points, such as position, mass, body forces and tractions, is temporarily transferred to the nodes of the computational background mesh. The material points are distributed in the background elements. An initial local position is assigned to each material point p inside the parent element. The global position $\mathbf{x}_p$ of every material point is calculated as:

$$\mathbf{x}_p \approx \sum_{i=1}^{n_{en}} N_i(\xi_p)\mathbf{x}_i \tag{2}$$

where n_{en} is the number of nodes of the parent element, $N_i(\xi_p)$ is the shape function of node i that is evaluated at the local position ξ_p of material point p, and $\mathbf{x}_i$ is the global position of node i.

The material points inside the same element initially occupy equal portion of the element volume, therefore the initial volume associated with material point p is obtained as:

$$\Omega_p = \frac{1}{n_{ep}} \int_{\Omega_e} d\Omega \approx \frac{1}{n_{eq}} \sum_{q=1}^{n_{eq}} \omega_q |\mathbf{J}| \tag{3}$$

where n_{ep} and n_{eq} denote the number of material points and quadrature points (Gauss points) in the element, respectively, ω_q

Please cite this article in press as: Tehrani FS et al. Comparison of Press-Replace Method and Material Point Method for analysis of jacked piles. Comput Geotech (2016), http://dx.doi.org/10.1016/j.compgeo.2016.04.017

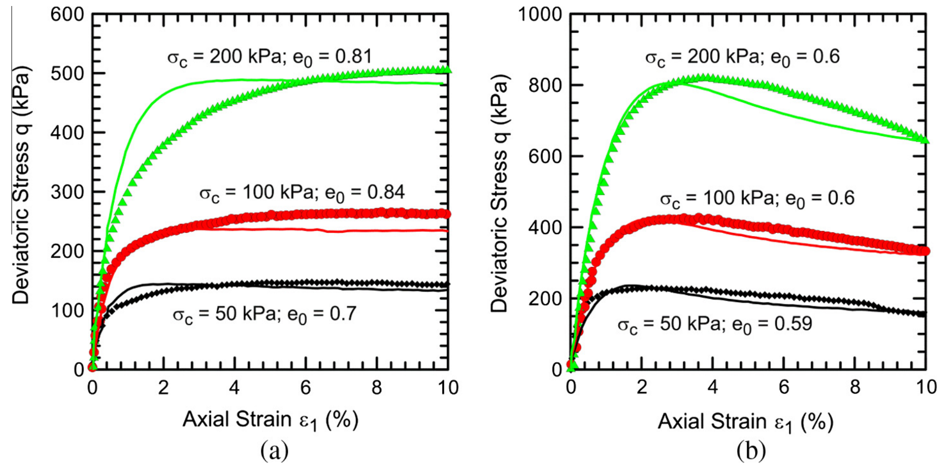

Fig. 3. Drained triaxial compression tests on: (a) loose sand and (b) dense sand.

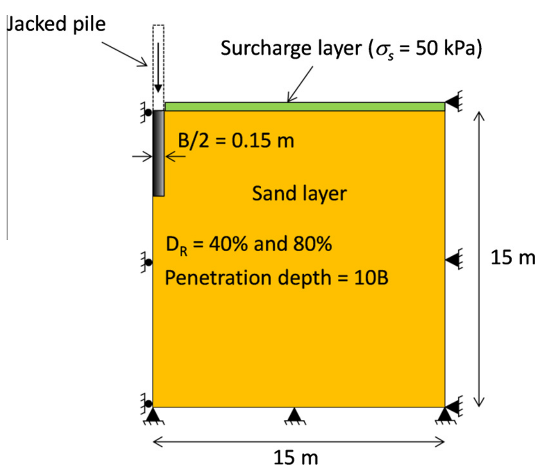

Fig. 4. Geometry and properties of the axisymmetric soil-pile model.

is the integration weight of Gauss point q, and $\mathbf{J}$ is the Jacobian matrix.

The mass of the material point is determined by the volume Ω_p of the element it occupies and its density ρ_p:

$$m_p = \Omega_p \rho_p \tag{4}$$

The gravity (body) force applied on the material point is given as:

$$\mathbf{f}_p^{gravity} = m_p \mathbf{g} \tag{5}$$

where $\mathbf{g}$ is the gravitational acceleration vector.

During the Lagrangian step, the computational mesh is used to determine the incremental solution of the field equations by integrating Eq. (1) over the time span t to $t + \Delta t$ using the Euler forward explicit scheme. First, the nodal mass at time t is computed by mapping the mass of the material point to the associated element node:

$$m_i^t \approx \sum_{p=1}^{n_{ep}} m_p N_i(\xi_p^t) \tag{6}$$

The nodal momentum at time t is calculated as:

$$m_i^t \mathbf{v}_i^t \approx \sum_{p=1}^{n_{ep}} m_p N_i(\xi_p^t) \mathbf{v}_p^t \tag{7}$$

where $\mathbf{v}_i^t$ is the velocity vector of node i at time t.

The traction force (if applicable) of node i at time t is given by:

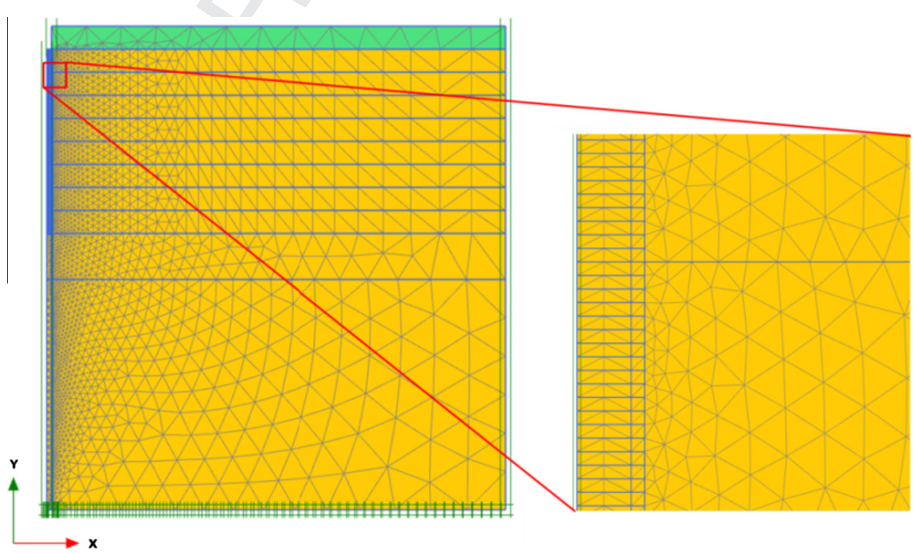

Fig. 5. 2D axisymmetric mesh used for PRM analyses.

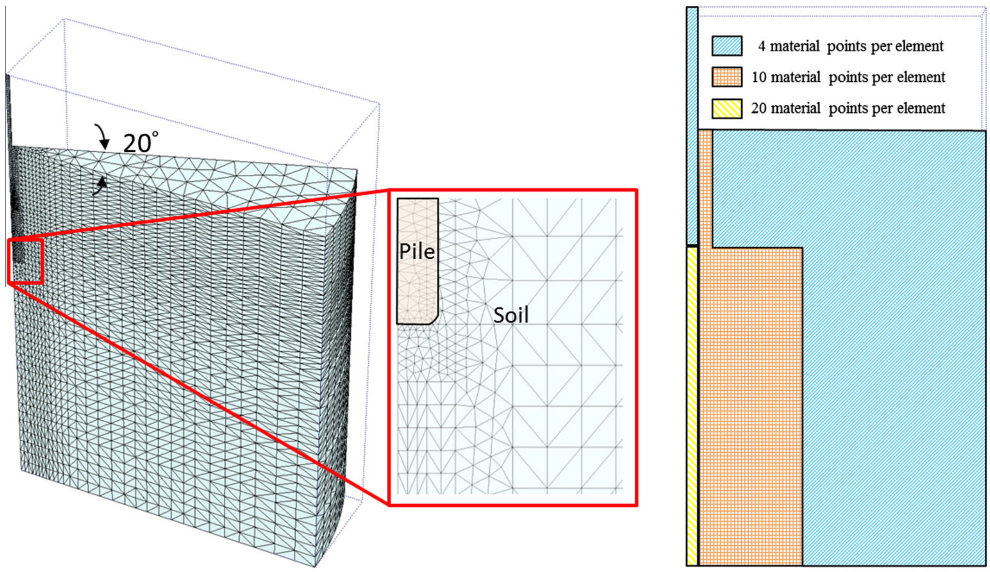

Fig. 6. Mesh discretization and the distribution of material points in MPM analyses.

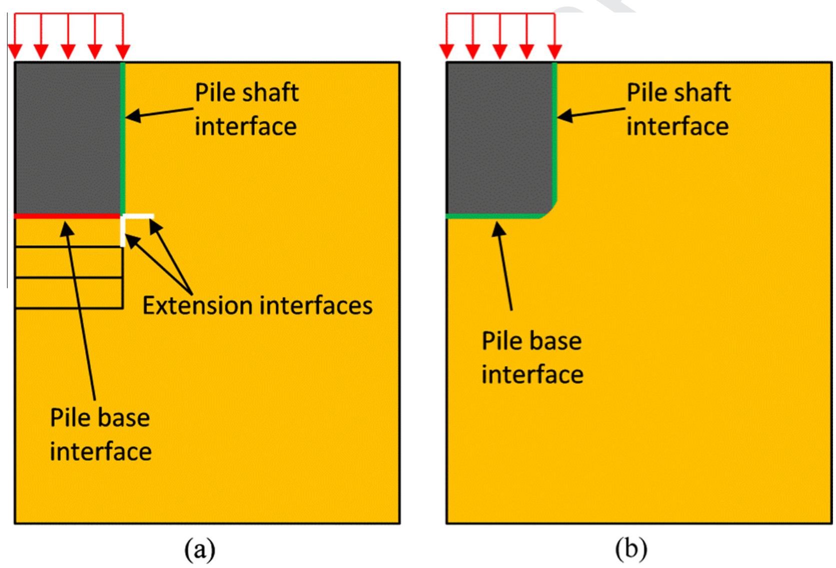

Fig. 7. Interface elements surrounding the jacked pile: (a) PRM and (b) MPM.

$$\mathbf{f}_i^{traction,t} = \sum_{p=1}^{n_{ebp}} N_i(\xi_p^t)\tilde{\mathbf{f}}_p^{traction}\left(\xi_p^t\right) \tag{8}$$

where n_{ebp} denotes the number of boundary particles inside the element that is located next to the loaded surface and $\tilde{\mathbf{f}}_p^{traction}$ is the traction force assigned to material point p.

The gravity force applied on node i at time t is calculated as:

$$\mathbf{f}_i^{gravity,t} \approx \sum_{p=1}^{n_{ebp}} N_i\left(\xi_p^t\right)\mathbf{f}_p^{gravity} \tag{9}$$

and the internal force as:

$$\mathbf{f}_i^{internal,t} = \sum_{p=1}^{n_{ep}} \Omega_p \boldsymbol{\sigma}_p^t \nabla N_i\left(\xi_p^t\right) \tag{10}$$

where $\boldsymbol{\sigma}_p^t$ is the stress tensor of material point p at time t and ∇ is the differential operator applied on N_i.

The nodal force at time t can then be computed as:

Table 4
Pile shaft interface properties.

D_R (%)	$E_{oed,i}$ (kPa)	$c_{ref,i}$ (kPa)	δ_i (°)	ψ_i (°)
40	60876.34	0	27.5	0
80	179874.9			

$$\mathbf{f}_i^t = \mathbf{f}_i^{traction,t} + \mathbf{f}_i^{gravity,t} - \mathbf{f}_i^{internal,t} \tag{11}$$

which is used to calculate the nodal acceleration vector:

$$\mathbf{a}_i^t = \mathbf{f}_i^t / m_i^t \tag{12}$$

Having the nodal properties calculated, it is now possible to calculate the properties of material points and element nodes at time $t + \Delta t$. First, the velocity of the material point at time $t + \Delta t$ is updated:

$$\mathbf{v}_p^{t+\Delta t} = \mathbf{v}_p^t + \sum_{i=1}^{n_{en}} \Delta t N_i(\xi_p^t)\mathbf{a}_i^t \tag{13}$$

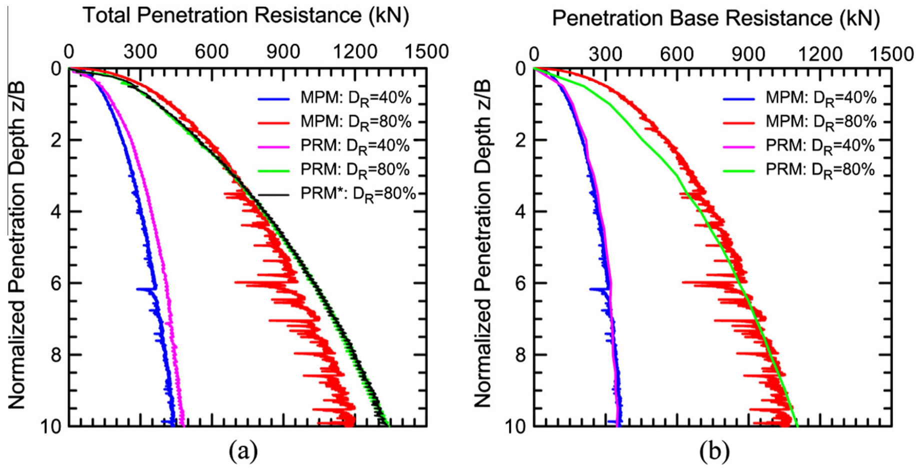

Fig. 8. Penetration resistance during the pile installation: (a) total resistance and (b) base resistance.

which is followed by updating the nodal velocity:

$$\mathbf{v}_i^{t+\Delta t} = m_i^{t,-1} \sum_{p=1}^{n_{en}} m_p N_i(\xi_p^t) \mathbf{v}_p^{t+\Delta t} \tag{14}$$

Then, the nodal incremental displacement is calculated as:

$$\Delta \mathbf{u}_i^{t+\Delta t} = \Delta t \mathbf{v}_i^{t+\Delta t} \tag{15}$$

that is used to update the position of the material point at time $t + \Delta t$.

$$\mathbf{x}_p^{t+\Delta t} = \mathbf{x}_p^t + \sum_{i=1}^{n_{en}} N_i(\xi_p^t) \Delta \mathbf{u}_i^{t+\Delta t} \tag{16}$$

Next, the strain increment and stress of the material point is updated:

$$\Delta \boldsymbol{\varepsilon}_p^{t+\Delta t} = \mathbf{B}(\xi_p^t) \Delta \mathbf{u}_p^{t+\Delta t} = \mathbf{B}(\xi_p^t)(\mathbf{x}_p^{t+\Delta t} - \mathbf{x}_p^t) \tag{17}$$

$$\boldsymbol{\sigma}_p^t \xrightarrow[\text{constituitive relation}]{\Delta \varepsilon_p^{t+\Delta t}} \boldsymbol{\sigma}_p^{t+\Delta t} \tag{18}$$

where $\Delta \boldsymbol{\varepsilon}_p^{t+\Delta t}$ is the incremental strain of material point p.

Next, the volume associated with the material point p is updated:

$$\Omega_p^{t+\Delta t} = (1 + \Delta \varepsilon_{vol,p}^{t+\Delta t}) \Omega_p^t \tag{19}$$

where $\Delta \varepsilon_{vol,p}^{t+\Delta t}$ is the incremental volumetric strain at time $t + \Delta t$ (summation of diagonal terms of the incremental strain tensor).

In the convective step, the computational mesh is either redefined or reset to its initial configuration while the material points maintain their state at the end of Lagrangian step. With the use of information carried by the material points, the solution can be reconstructed on any mesh. Therefore, the computational mesh can be chosen for convenience which is the great advantage of MPM. More details of the MPM analysis used in this study can be found in [33].

2.2. Press-Replace Method

The PRM is a simplified approach based on standard finite element (FE) method for simulating boundary-value problems that involves penetration of an object into a continuum. PRM was first introduced by [36] for simulating the load-controlled penetration of a suction anchor in clay. Recently, Engin [20] successfully used the displacement-controlled PRM to simulate pile and cone penetration in a sandy soil. In PRM, the initial mesh is preserved, while the material properties of the penetrated volume are updated at the beginning of each phase resulting in a change of the global stiffness matrix without the need for updating the mesh. This makes the calculations faster than large-deformation analysis techniques [20]. Despite its advantages, PRM has its own limitations, too; most importantly, it is unable to model the flow of the soil below the pile base and around peripheral zone of the penetrating pile.

PRM involves a step-wise geometry update, which consists of straining the phase followed by the geometry update. The purpose of the geometry update is to model the advancing part of the penetrating object (jacked pile in this study), which can be achieved by modifying the global stiffness matrix at the beginning of every replacement phase. At each calculation phase i, an updated global stiffness matrix and the associated boundary conditions are formed to solve a system of algebraic equations as:

$$\mathbf{K}^i \Delta \mathbf{u} = \Delta \mathbf{f}^i \tag{20}$$

The load increment $\Delta \mathbf{f}^i$ is equal to the total unbalance at the beginning of phase i as a result of the geometry update:

$$\Delta \mathbf{f}^i = \mathbf{f}_{ext}^i - \mathbf{f}_{int}^{i,0} \tag{21}$$

where $\mathbf{f}_{ext}^i$ is the external load vector at phase i. The internal reaction force vector $\mathbf{f}_{int}^{i,0}$ is calculated as:

$$\mathbf{f}_{int}^{i,0} = \int_{\Omega} \mathbf{B}^T \boldsymbol{\sigma}^{i,0} dV \tag{22}$$

where $\mathbf{B}^T$ is the matrix containing the derivatives of the shape functions and $\boldsymbol{\sigma}^{i,0}$ is the stress state at the beginning of phase i.

PRM consists of applying a Dirichlet boundary condition (displacement) at every phase. The displacement boundary condition is applied on top of the pile to push the pile downward. The whole displacement-controlled FE analysis resembles a staged construction process. Fig. 2 illustrates three sequential phases in PRM.

As shown in Fig. 2, the penetration path is divided into several slices of thickness t_s. When the pile base (in gray color) is resting on top of slice i, the displacement-controlled axial loading of u_i, equal to the summation of previous displacement and an additional displacement increment, is applied on the pile head. The displacement increment is equal to the thickness of the soil slice t_s. Once the loading stage (i.e., press) is completed, the soil material in slice i is replaced by the pile material (i.e., replace). This process continues until the pile base reaches to the last slice on the penetration path. PRM is performed within the framework of the small-deformation theory (infinitesimal strain), in which the global stiffness matrix is always formed based on the original (undeformed)

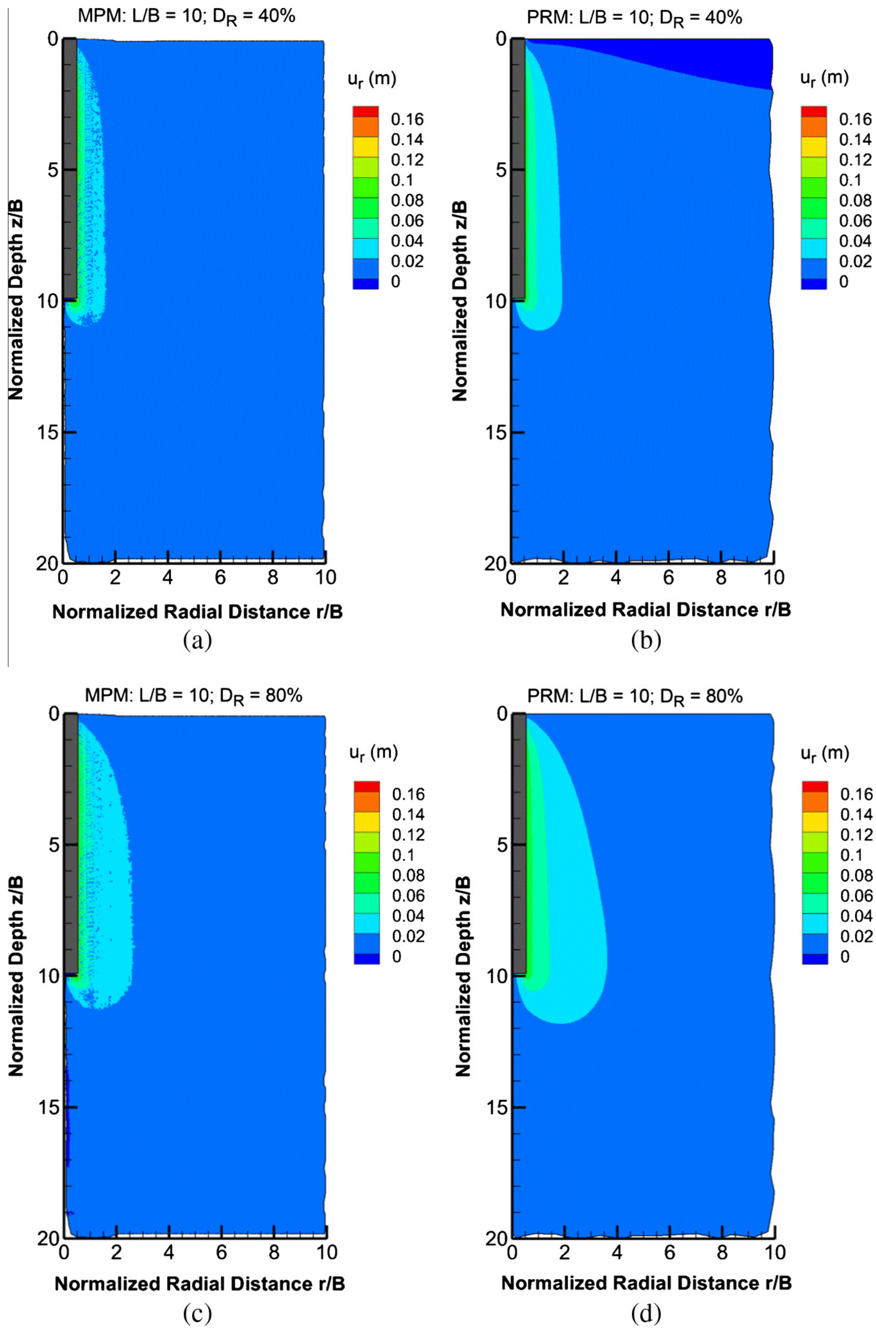

Fig. 9. Radial displacement after 10*B* pile penetration: (a) MPM in the loose sand, (b) PRM in the loose sand, (c) MPM in the dense sand, and (d) PRM in the dense sand.

geometry of the soil-pile model. In other words, the global stiffness matrix only takes into account the updated material properties in the clusters (slices) that have switched to the pile material. It is noted that in the replace stage, a thin slice of soil is replaced by stiffer elastic material (pile). Therefore, there should be some compensation in the form of straining inside and near the zone that is replaced by the pile material. However, this straining is not achieved in PRM, which relies on small deformation theory, because the amount of the elastic energy is very small compared to the total energy that is spent in the system. The total spent energy is mostly dissipated due to plastic deformation. Therefore, this small compensation of straining is not required. Hence, by not incorporating this straining the amount of the dissipated energy is slightly overestimated. More details about PRM can be found in [20].

3. Analysis preliminaries

3.1. Material

The granular material used in the analyses presented in the current paper is known as Baskarp sand, which is a sand with angular to sub-angular grains. Basic properties of Baskarp sand are listed in Table 1.

The pile material is assumed linear elastic with Young's modulus of E_p = 30 GPa and Poisson's ratio of ν_p = 0.3.

3.2. Constitutive model

The hypoplastic soil model (hereafter referred to as HP) developed by von Wolffersdorff [38] and its small strain extension by

Please cite this article in press as: Tehrani FS et al. Comparison of Press-Replace Method and Material Point Method for analysis of jacked piles. Comput Geotech (2016), http://dx.doi.org/10.1016/j.compgeo.2016.04.017

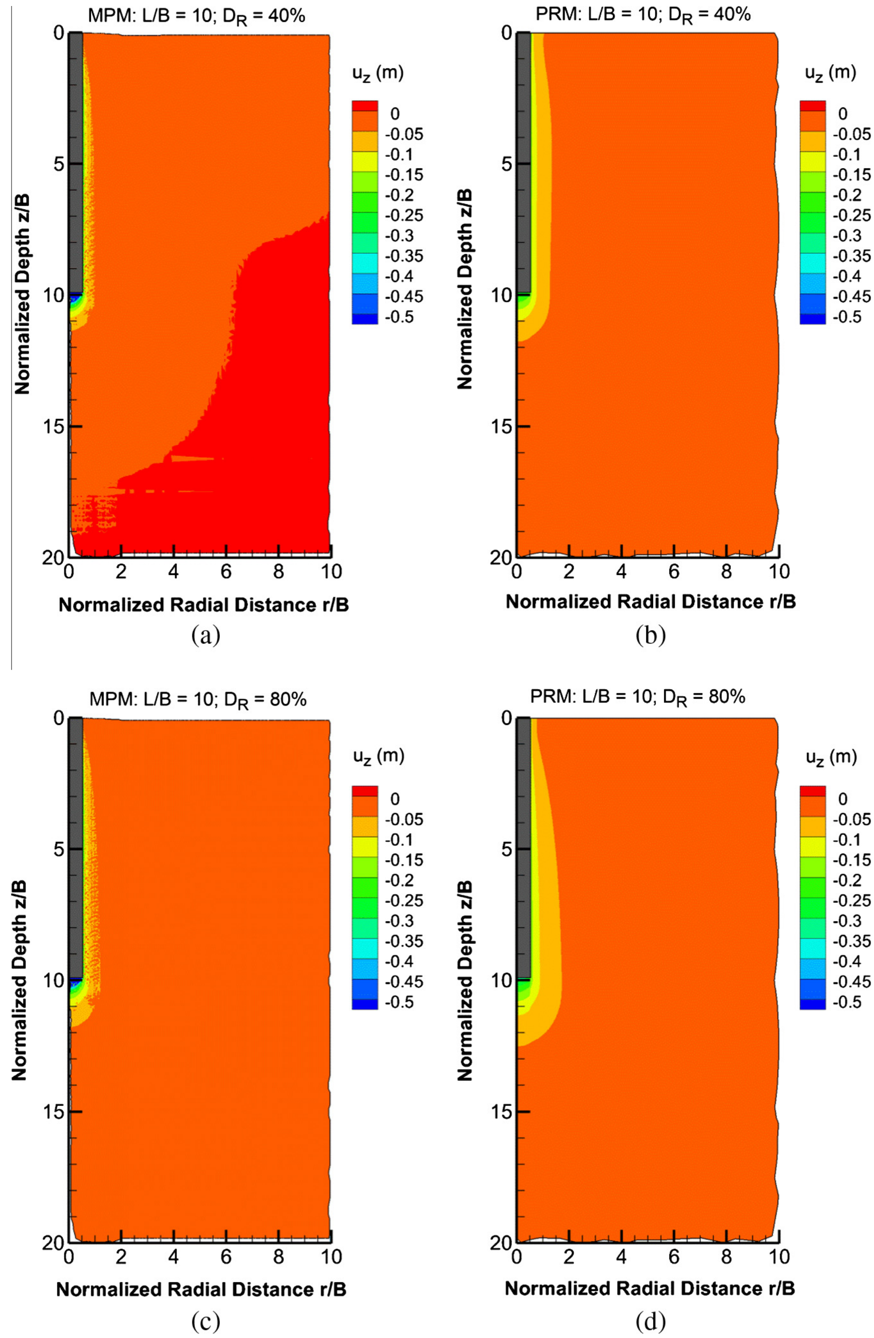

Fig. 10. Vertical displacement after 10B pile penetration: (a) MPM in the loose sand, (b) PRM in the loose sand, (c) MPM in the dense sand, and (d) PRM in the dense sand.

Niemunis and Herle [39] were used in this paper due to their potential for realistic prediction of the sand behavior during pile installation and pile loading. The HP model is able to capture the strain- and stress-dependent responses of sand and accounts for the dependency of the soil response on the stress path. The model can predict the change in the void ratio (and hence the density) as well as the change in the stiffness and strength of the sand during loading and unloading. The HP model incorporates the Matusoka–Nakai failure criterion coupled with Runge–Kutta–Fehlberg explicit adaptive integration scheme with local sub-stepping [40]. Calibration parameters of the HP model for Baskarp sand are shown in Tables 2 and 3.

The drained triaxial compression results of Baskarp sand along with the numerical simulation of the associated element tests are shown in Fig. 3.

To avoid convergence issues, the small strain extension of the HP model was not employed in the PRM simulation of the jacking processes; however it was used for the load-settlement analysis of the jacked pile.

3.3. Modeling considerations

3.3.1. Cases analyzed

Continuous jacking (single stroke) of a circular-cross-section pile, with the diameter $B = 0.3$ m, into uniform Baskarp sand is considered in this paper. Fig. 3 shows the problem studied.

As shown in Fig. 4, a thin elastic layer is considered on top of the sand layer to avoid numerical issues due to the tension developed at the surface of the sand layer during the installation process.

Please cite this article in press as: Tehrani FS et al. Comparison of Press-Replace Method and Material Point Method for analysis of jacked piles. Comput Geotech (2016), http://dx.doi.org/10.1016/j.compgeo.2016.04.017

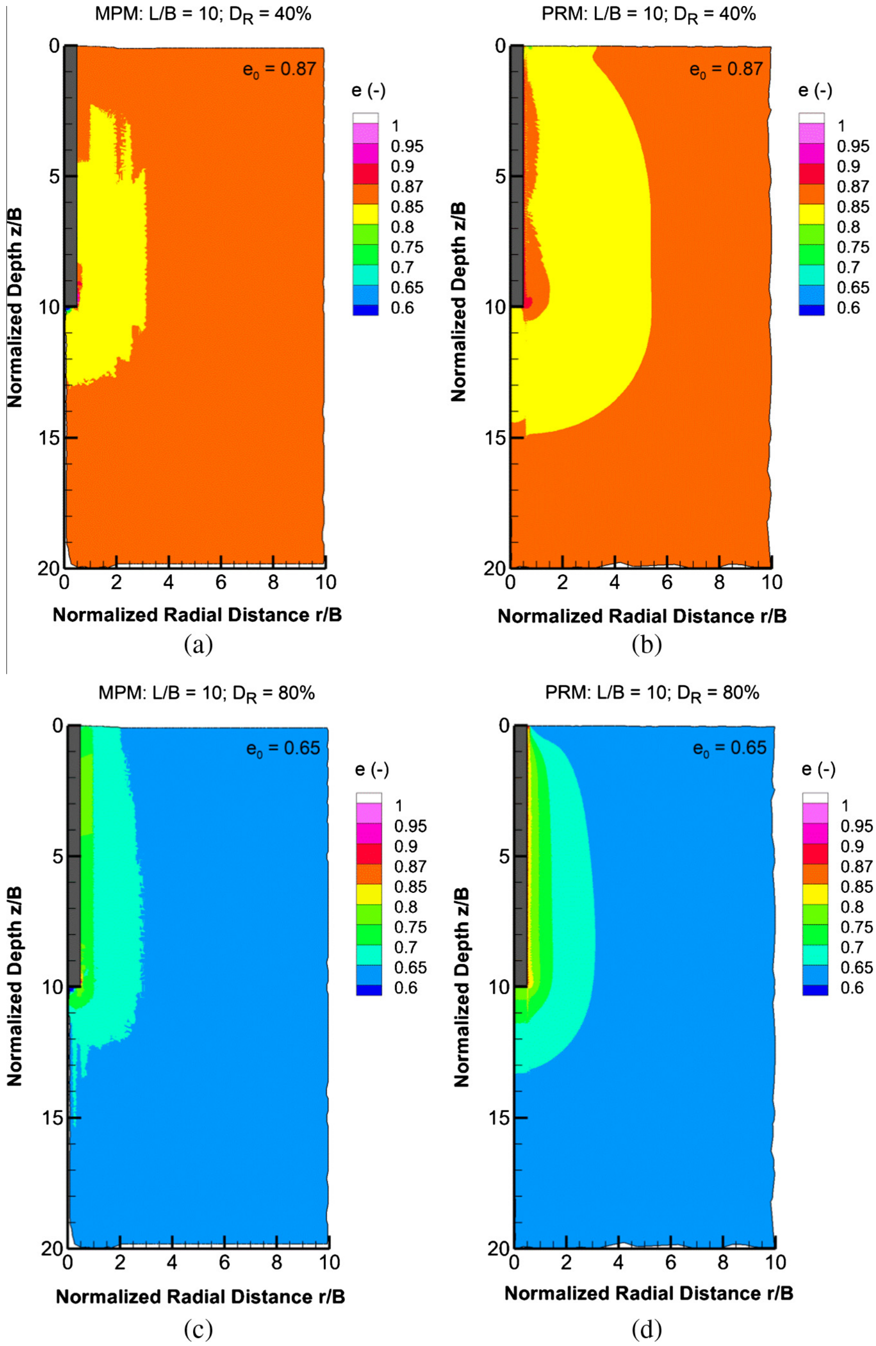

Fig. 11. Void ratio after 10*B* pile penetration: (a) MPM in the loose sand, (b) PRM in the loose sand, (c) MPM in the dense sand, and (d) PRM in the dense sand.

In this paper, MPM is assumed as the reference method for the analysis of jacked piles. The accuracy of the method was verified in Phuong et al. [41] by comparing the results of MPM analysis with centrifuge modeling of jacked piles in Baskarp sand, which is the sand used in this study as well.

3.3.2. PRM analysis

Due to the axisymmetric nature of the analyzed boundary-value problem, PRM analyses are performed under axisymmetric conditions using PLAXIS 2D [42]. 15-node triangular elements are used to discretize the soil-pile domain to increase the accuracy of the numerical solution. The mesh is refined around the pile (see Fig. 5) to closely capture the response of soil during jacking. Since the pile penetration in PRM is a displacement-controlled process, the arc-length control method is not used in the PLAXIS analyses. The minimum and maximum desired iterations are set to 6 and 15, respectively. This implies that if the number of iterations used for convergence in a certain loading step is more than 15, the step size will be halved. Conversely, if the number of iterations required for convergence is less than 6, the loading step size is doubled. The global tolerated error is set to 1% which is a standard accuracy criterion in Plaxis.

In the PRM analyses, the thickness of the soil slices is set to $t_s = 0.03$ m (=$B/10$) which is equal to the axial displacement

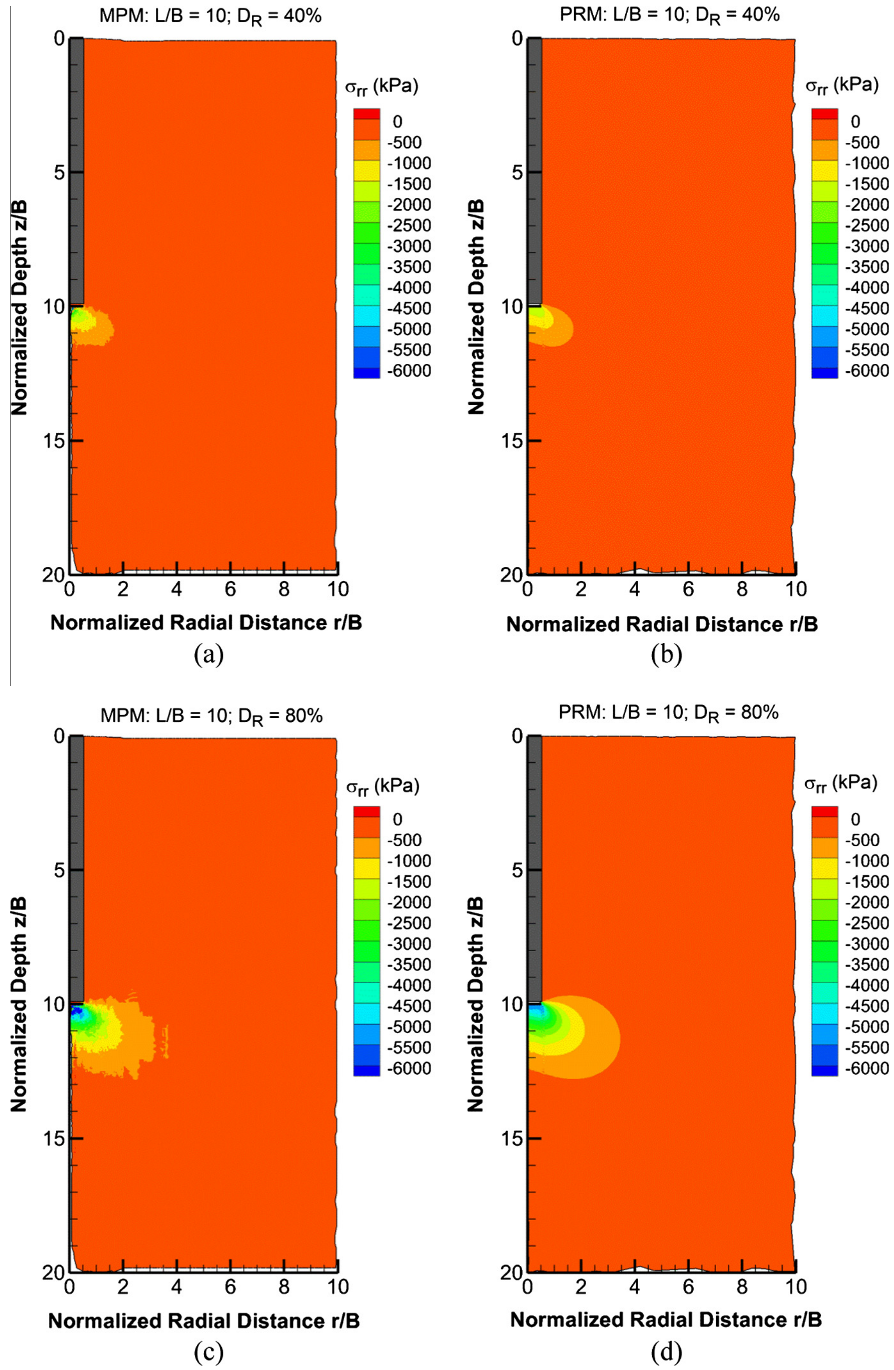

Fig. 12. Radial stress after 10B pile penetration: (a) MPM in the loose sand, (b) PRM in the loose sand, (c) MPM in the dense sand, and (d) PRM in the dense sand.

increments used in the pile jacking. Engin [20] reported that the slice thickness ranged from $B/10$ to $B/8$ is an optimal thickens for soil slices considered in PRM.

3.3.3. MPM analysis

In the MPM analyses, a 20° slice of the soil-pile domain is used (see Fig. 6). As shown in Fig. 6, the soil domain is divided into three zones where 4, 10, and 20 material points are assigned to four-node tetrahedral elements used in the background mesh.

More material points are assigned to elements in zones that are expected to undergo more deformation. The pile is modeled as a rigid body penetrating into the soil at the rate of 0.02 m/s. Although the shape of the pile tip is flat, the corner of the pile tip in the simulation is slightly curved to avoid numerical difficulties due to stress singularity at the pile tip corner. The MPM analyses are performed using an in-house code of the MPM Research Community, which is contributed by the University of Cambridge (UK), UPC Barcelona (Spain), TU Hamburg-Harburg (Germany) and Deltares (the Netherlands).

3.3.4. Interface elements

Interface elements are introduced at the pile-soil interfaces to properly model the interaction between the pile and the soil (see Fig. 7). The interface elements are modeled using elastic-perfectly plastic Mohr–Coulomb model. In order to change the interface stiffness values either the interface virtual thickness or

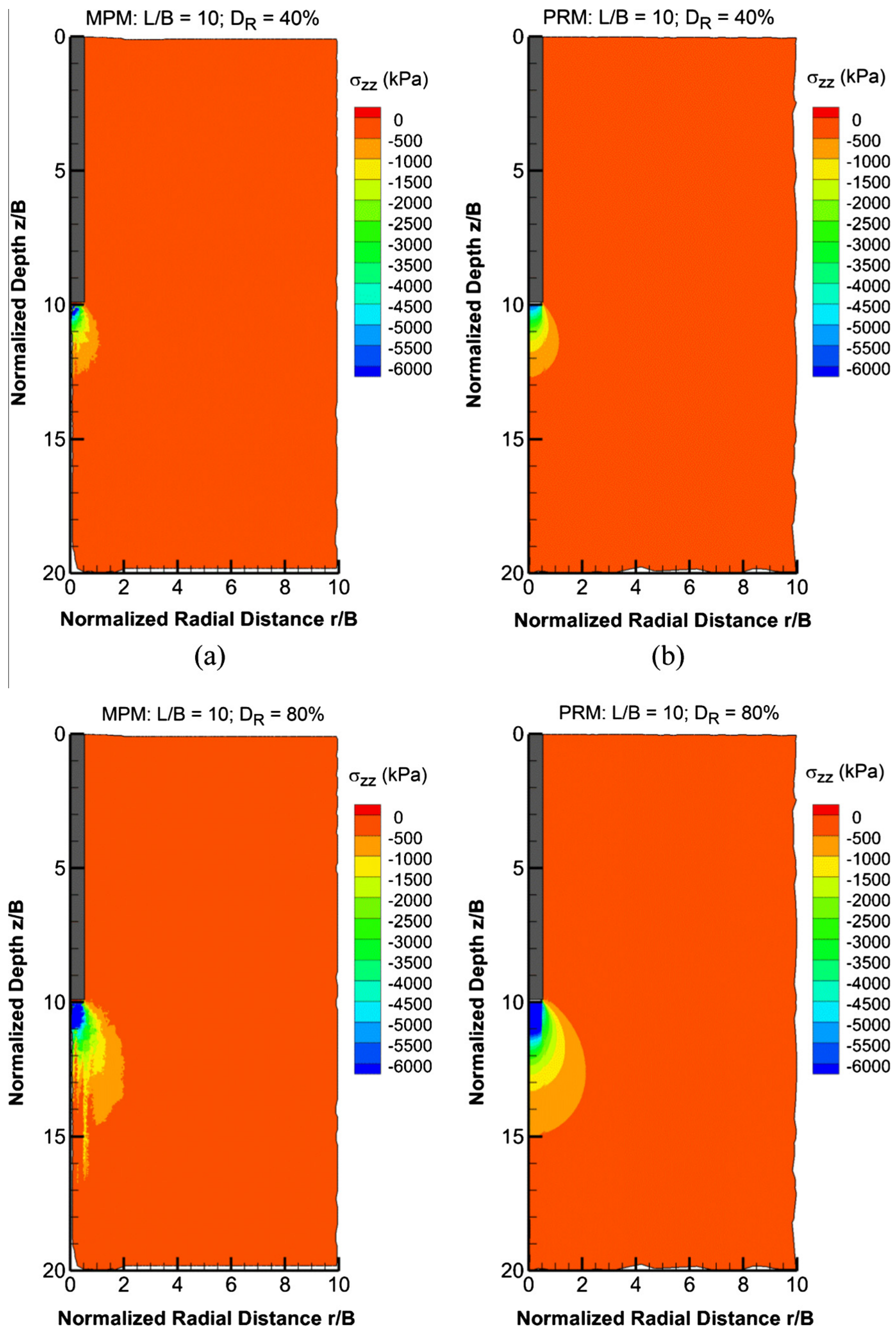

Fig. 13. Vertical stress after 10B pile penetration: (a) MPM in the loose sand, (b) PRM in the loose sand, (c) MPM in the dense sand, and (d) PRM in the dense sand.

the interface shear stiffness, G_i (hence the interface oedometric stiffness $E_{oed,i}$) has to be modified. The Poisson's ratio of the interface elements is $\nu_i = 0.45$. The interface elements used in the analyses are described next.

The pile shaft is under an excessive shearing during the pile installation. Therefore, it is reasonable to assume that the critical state prevails at the pile shaft-soil interface. Since the surface of jacked piles has asperities smaller than the sand particles, the interface friction angle δ_c is normally assumed a fraction of the critical state friction angle ϕ_c of the nearby sand, which is independent of the soil initial density. Hence, the interface critical state friction coefficient is taken as 90% (reduction factor $R_i = 0.9$) of the critical state friction of the sand ($\tan\delta_c = 0.9\ \tan\phi_c$). Table 3 shows the properties used for the pile shaft interface element in the PLAXIS interface tab sheet.

The interface stiffness ($E_{oed,i}$) is calculated using the following equations.

$$G_i = R_i^2 G \tag{23}$$

$$E_{oed,i} = 2G_i \frac{1-\nu_i}{1-2\nu_i} \tag{24}$$

where G is the shear modulus of nearby soil and G_i is the shear modulus of the interface element. The effect of stiffness properties is purely numerical and should not affect the final result (see Table 4).

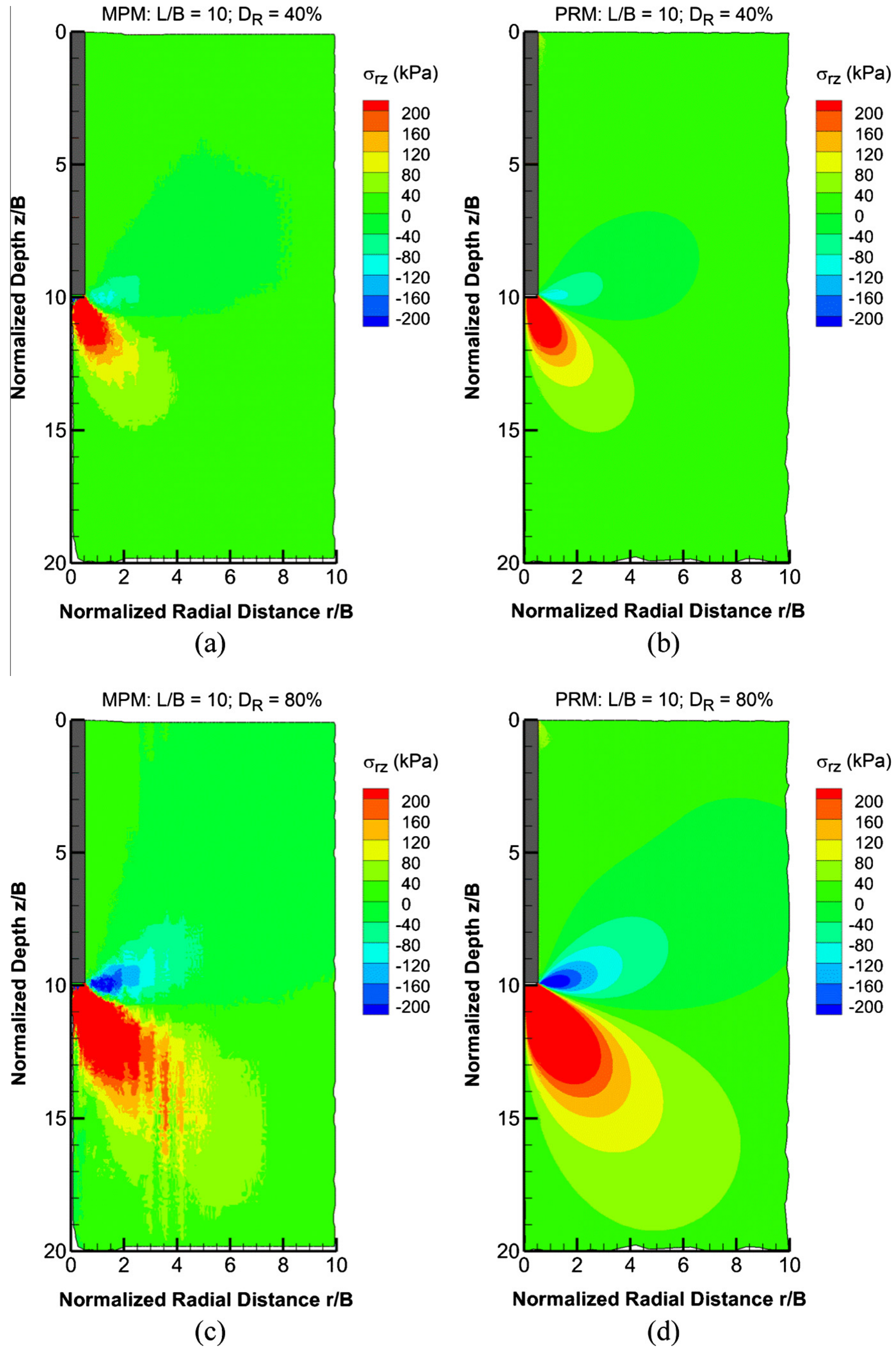

Fig. 14. Radial stress after 10B pile penetration: (a) MPM in the loose sand, (b) PRM in the loose sand, (c) MPM in the dense sand, and (d) PRM in the dense sand.

The pile base interface is under a large confining pressure. Therefore, it can be assumed that the critical state exists at the pile base-soil interface. Since there is no relative displacement between pile base and the soil in PRM, the interface friction angle is equal to the critical state friction angle of the soil ($R_i = 1$). However, to be consistent with the MPM analyses where only one type of interface elements could be used, the interface elements used in the shaft was also used for the base. It will be shown later that this decision did not affect the final results.

In PRM, interface elements at the pile base corner must be extended into the soil volume (see Fig. 7(a)), in order to avoid stress oscillations/singularity at the corner of the pile base [20]. In this study, the length of the horizontal and vertical extensions is equal to the soil slice thickness which is equal to 0.03 m, following recommendations in [20]. To avoid any relative slippage between the extended interface elements and the nearby soil and to ensure that the shear strength at the extension elements is always higher than the shear stress and to guarantee that the artificial interfaces extended in the soil do not fail or deform, it is necessary to adopt a high value for the reference cohesion $c_{ref,i}$(=1000 kPa). At the end of every loading (press) stage in PRM, the horizontal extension interface for that stage is switched off and the vertical extension interface is replaced by the shaft interface element at the next replacement stage. The oedometric stiffness of extension elements is calculated by taking $R_i = 1$ in Eq. (23).

4. Results and discussion

The pile was jacked down to 10B below the ground level. Fig. 8 shows the total penetration (installation) resistance and the base

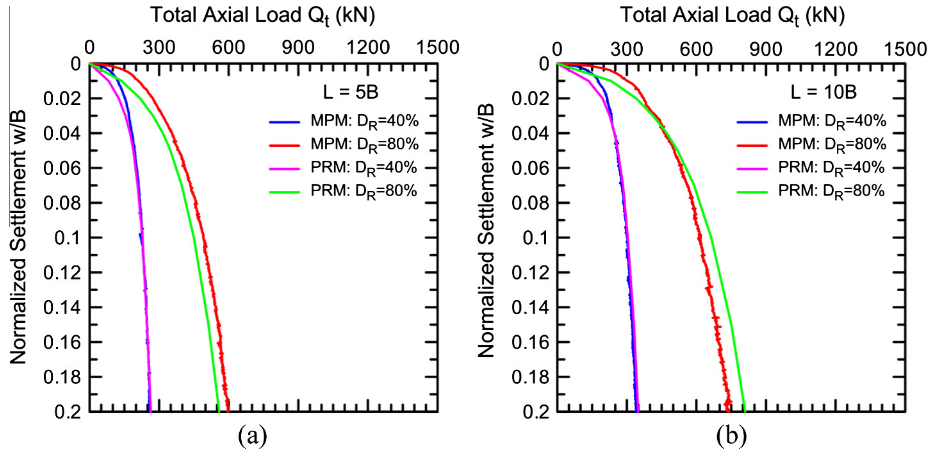

Fig. 15. Load-settlement response of the jacked pile in dense and loose sands: (a) $L = 5B$ and (b) $L = 10B$.

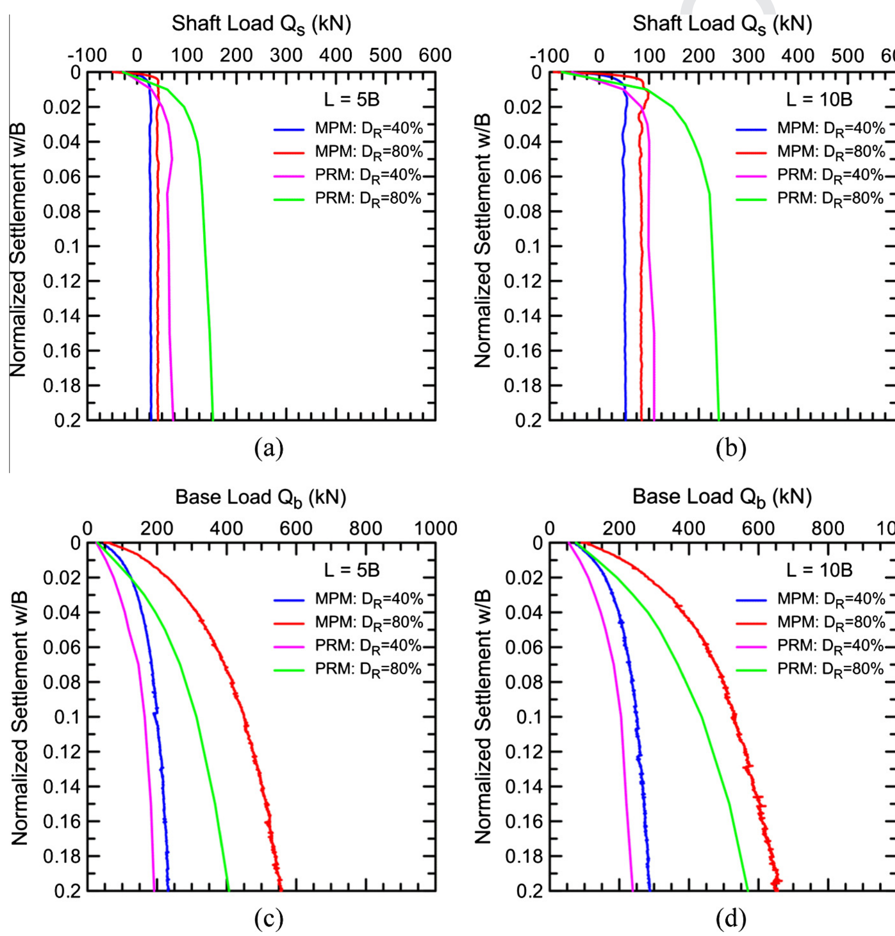

Fig. 16. Soil resistance during the numerical static load tests: (a) shaft resistance for $L = 5B$, (b) shaft resistance for $L = 10B$, (c) base resistance for $L = 5B$, and (d) base resistance for $L = 10B$.

resistance mobilized during the penetration for both PRM and MPM.

It is clear from Fig. 8 that, in general, the total jacking force and the mobilized base resistance computed using PRM are in good agreement with those calculated using MPM. The total jacking force, which is equal to the summation of the base and shaft resistances, obtained from PRM is slightly higher (8–14%) than MPM; given that the base resistances from PRM and MPM are very close, it is clear that the shaft resistance obtained from PRM during the pile installation is greater than the one obtained from MPM.

To explore the effect of interface friction at the pile base on the penetration resistance calculated using PRM, an additional analysis with the base interface friction angle of 30° was performed for the dense sand, which is labeled PRM* in Fig. 8(a). It is shown in Fig. 8(a) that altering the base interface friction angle from 27.5° to 30° has an immaterial effect on the penetration resistance (the

Please cite this article in press as: Tehrani FS et al. Comparison of Press-Replace Method and Material Point Method for analysis of jacked piles. Comput Geotech (2016), http://dx.doi.org/10.1016/j.compgeo.2016.04.017

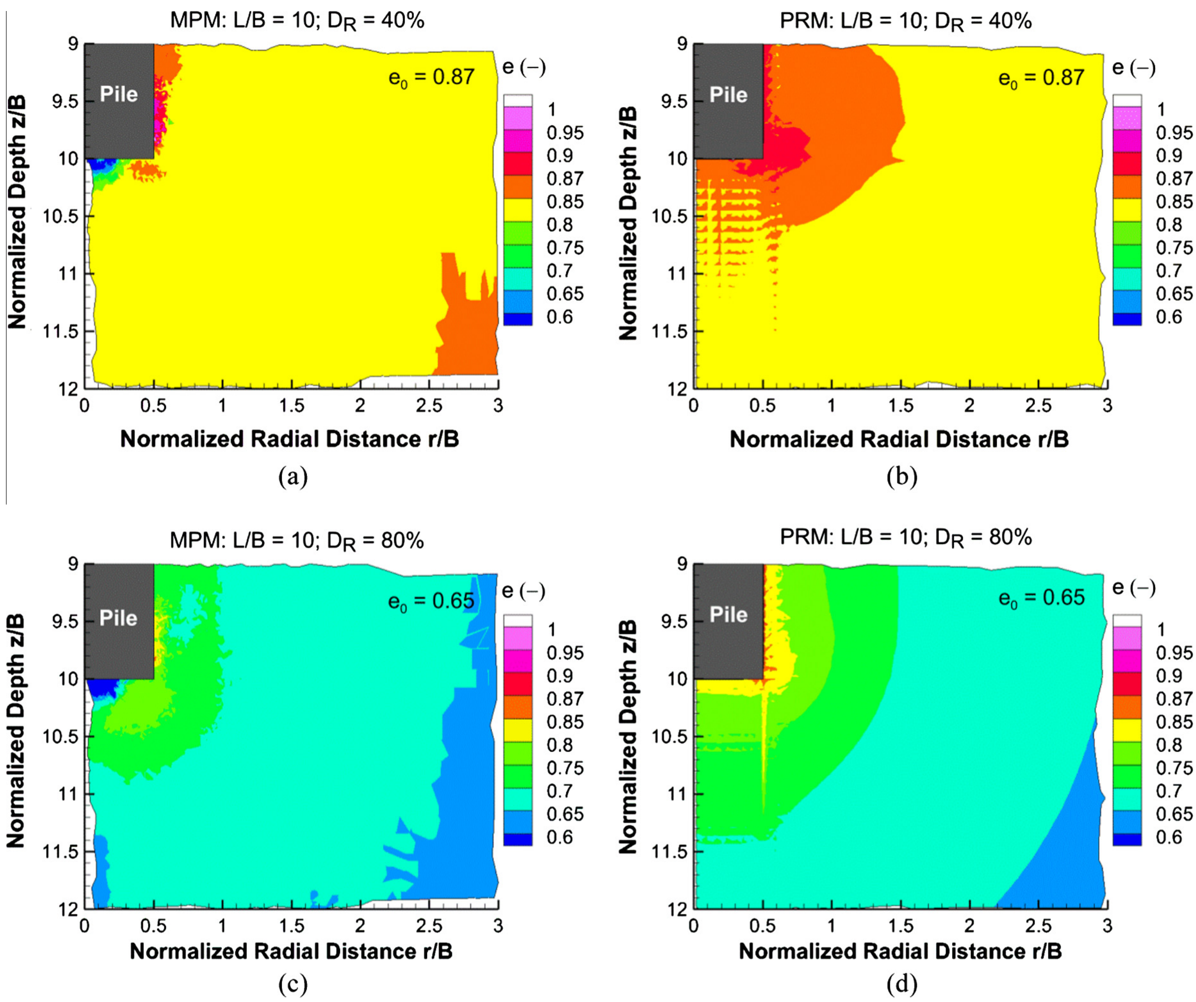

Fig. 17. Void ratio around the pile base after unloading of 10*B*-long pile: (a) MPM in the loose sand, (b) PRM in the loose sand, (c) MPM in the dense sand, and (d) PRM in the dense sand.

associated plots overlap each other), which warrants the use of one interface friction angle at the pile-soil interface for all analyses presented in this paper.

Figs. 9–14 illustrate the radial displacement, vertical displacement, void ratio, radial stress, vertical stress and shear stress across the soil domain at the end of 10*B*-deep pile jacking.

It is shown in Fig. 9 that as the soil becomes denser the soil extent that undergoes the same radial displacement (for example $u_r = 0.02$ m) becomes greater in PRM than in MPM.

Fig. 10 shows that the same observation made for the radial displacement holds for the vertical displacement, too. However, it is shown that in MPM simulation the maximum vertical displacement right below the pile base is greater than PRM.

As shown in Fig. 11, a greater part of the domain of the loose sand undergoes compaction ($e < e_0$) in PRM analysis than in MPM analysis. For the dense sand, both methods show clear soil dilation next to the pile shaft ($e > e_0$), with PRM resulting in more dilation right next to the pile shaft than MPM. This difference between MPM and PRM is the major reason behind predicting higher installation shaft resistance by PRM in comparison with MPM.

Figs. 12–14 show the similarity of the radial, vertical and shear stresses around the pile base in PRM and MPM. This explains the similar base resistances observed in Fig. 8(a).

Once the installation is complete, the pile is unloaded. Then, a numerical static load test (SLT) is performed where a displacement-controlled loading is applied to the pile head until the pile head vertical displacement reaches 0.2*B*. Fig. 15 shows the load-settlement response of the jacked piles installed in the loose and dense sands. The numerical SLTs were performed on piles of length 5*B* and 10*B* to show the effect of pile length on the load-settlement response of jacked piles and the predictions made by PRM and MPM.

As shown in Fig. 15, the load settlement responses obtained from PRM and MPM are in good agreement for the piles installed in the loose sand, while for the piles installed in the dense sand the load predicted by PRM for 0.2*B* pile head settlement in the dense sand is ≈9% higher and ≈6% lower than the MPM for the pile length of 10*B* and 5*B*, respectively (though these differences are, practically speaking, trivial).

For further analysis, the shaft and base resistance mobilized during the numerical SLTs are shown separately in Fig. 16.

Fig. 16 reveals that the shaft resistance calculated using PRM is greater than MPM and the base resistance calculated using PRM is lower than MPM. The lower base resistance and higher shaft resistance of PRM counterbalance each other which results in the total resistance that is in good agreement with that of MPM (see Fig. 15). The higher shaft resistance predicted by PRM during the SLTs is consistent with what was observed during the pile installation: in both cases, PRM results in higher shaft resistances. The base resistance obtained from PRM was in close agreement with that of MPM during pile installation, whereas for the SLTs, it is lower than MPM. The reason for this inconsistency is that during the

Please cite this article in press as: Tehrani FS et al. Comparison of Press-Replace Method and Material Point Method for analysis of jacked piles. Comput Geotech (2016), http://dx.doi.org/10.1016/j.compgeo.2016.04.017

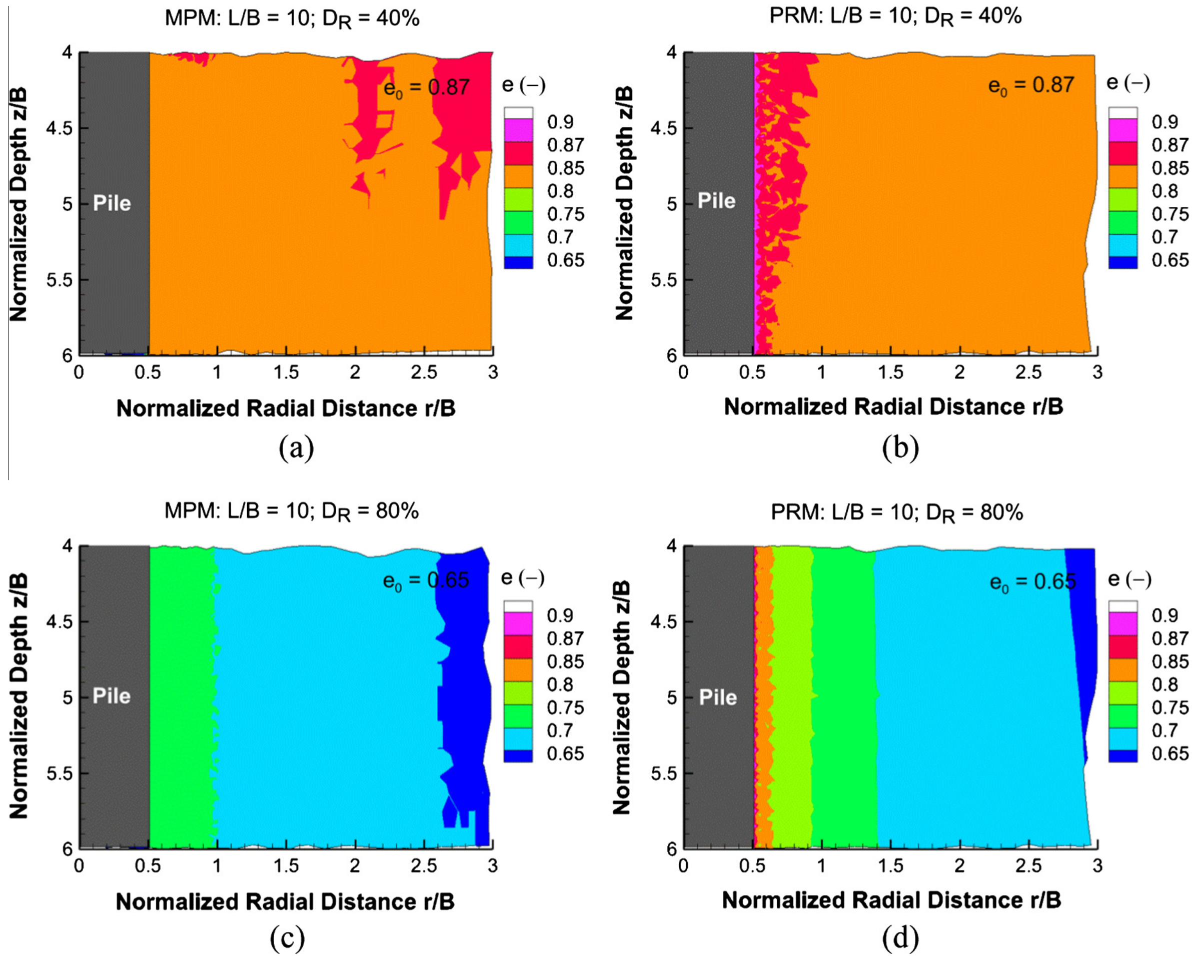

Fig. 18. Void ratio near the pile shaft after unloading of 10*B*-long pile: (a) MPM in the loose sand, (b) PRM in the loose sand, (c) MPM in the dense sand, and (d) PRM in the dense sand.

installation as the vertical displacement of the pile increases the stiffness matrix of the soil-pile domain is continually modified in PRM (soil slice below the pile tip is replaced by the pile material), while in the SLTs this change in the stiffness matrix does not take place. Therefore, the initial stiffness matrix is associated with the soil state at the end of pile unloading after installation. The small-strain theory demands that pile material does not move downward during the SLTs, while in MPM the pile is literally moving downward during the SLT process.

The difference in the shaft and base resistances of PRM and MPM can be also attributed to the difference in the state of the soil at the very beginning of the static load tests. One of the parameters that quantifies the state of the soil in this study is the sand void ratio. Fig. 17 shows the void ratio around the pile base ($2B$ below the pile base and $3B$ away radially from the pile centerline) in the loose and dense sands after unloading the pile at the end of pile installation. It is seen in Fig. 17 that in MPM there is a clear compaction below the pile base in both loose and dense sands after pile unloading, whereas in PRM this soil compaction is not significant in the loose sand and there is no sign of soil compaction below the pile base in the dense sand. Therefore, it is reasonable to observe higher base resistance in the numerical SLT results of MPM and lower base resistance from those of PRM.

To explain the notable difference in the shaft resistance obtained from PRM and MPM, the void ratio near the pile shaft at the mid length of the pile ($z = 4B$ to $6B$ for $L = 10B$) upon pile unloading is plotted in Fig. 18.

Fig. 18(a) shows that in MPM analysis, there is a contraction near the pile shaft installed in the loose sand, while according to Fig. 18(b), PRM analysis results in a slight dilation near the shaft of the pile installed in the loose sand. In the dense sand (Fig. 18(c) and (d)), both MPM and PRM analyses result in soil dilation near the pile shaft with PRM producing more dilation than MPM. These differences in the state of void ratio next to the pile shaft after unloading clearly explain why PRM produces higher shaft resistance than MPM during the numerical SLTs.

5. Summary and conclusions

In this study, the installation of jacked piles in loose and dense sands was simulated using Press-Replace Method (PRM) and Material Point Method (MPM) and the results were compared. The sand was modeled using a hypoplastic constitutive model. It was shown that during pile installation PRM can produce jacking force and base resistance that are very close to the jacking force and base resistance obtained from MPM. Also, it was concluded that in comparison with MPM, PRM results in lower base resistance and higher shaft resistance during pile operational loading (e.g., SLT). At the operational loading stage, PRM simulates a small-strain BVP with the assumption that the geometry of the pile-soil system does not change. But, in MPM, the pile indeed further penetrates into the soil and therefore benefits from increase in the soil bearing capacity due to this penetration. Thus, it can be suggested that

PRM yields a conservative base resistance at the operational loading stage in comparison with MPM. The higher shaft resistance and lower base resistance from PRM counterbalance each other and result in the total capacity that is very close to the one predicted by MPM.

Acknowledgements

This research is supported by the Dutch Technology Foundation STW (grant no. 10189), which is the applied science division of NWO, and the Technology Program of the Ministry of Economic Affairs. The research leading to these results has also received funding from the 7th Framework Program of European Commission (FP7/2007-2013 under grant agreement PIAG-GA-2009-230638). The authors are grateful for these supports. The findings reflect only the authors' views and the supporting agencies are not liable for any use that may be made of the information contained therein.

References

[1] Basu P, Loukidis D, Prezzi M, Salgado R. Analysis of shaft resistance of jacked piles in sands. Int J Numer Anal Methods Geomech 2011;35:1605–35.
[2] Yang J, Tham LG, Lee PK, Yu F. Observed performance of long steel H-piles jacked into sandy soils. J Geotech Geoenviron Eng 2006;132:24–35.
[3] Babushkin GU, Ginzburg LK. Strengthening of foundations on collapsible soils by means of jacked piles. Soil Mech Found Eng 1984;21:14–20.
[4] Cooke RW, Price G, Tarr K. Jacked piles in London Clay: a study of load transfer and settlement under working conditions. Géotechnique 1979;29:113–47.
[5] Lehane BM, Jardine RJ, Bond AJ, Frank R. Mechanisms of shaft friction in sand from instrumented pile tests. J Geotech Eng 1993;119:19–35.
[6] Chow FC. Field measurements of stress interactions between displacement piles in sand. Gr Eng 1995;28:36–40.
[7] White DJ, Bolton MD. Displacement and strain paths during plane-strain model pile installation in sand. Geotechnique 2004;54:375–97.
[8] White DJ, Lehane BM. Friction fatigue on displacement piles in sand. Géotechnique 2004;54:645–58.
[9] Dijkstra J, Broere W, van Tol AF. Experimental investigation into the stress and strain development around a displacement pile. In: Proc Tenth Int Conf Piling Deep Found. p. 252–9.
[10] Arshad M, Tehrani FS, Prezzi M, Salgado R. Experimental study of cone penetration in silica sand using digital image correlation. Geotechnique 2014;64:551–69.
[11] Susila E, Hryciw RD. Large displacement FEM modelling of the cone penetration test (CPT) in normally consolidated sand. Int J Numer Anal Methods Geomech 2003;27:585–602.
[12] Dijkstra J, Broere W, Heeres OM. Numerical simulation of pile installation. Comput Geotech 2011;38:612–22.
[13] Engin HK, Brinkgreve RBJ, van Tol AF. On the numerical modelling and incorporation of installation effects of jacked piles: a practical approach. In: Hicks M, editor. Install Eff Geotech Eng; 2013. p. 104–10.
[14] Liyanapathirana DS. Arbitrary Lagrangian Eulerian based finite element analysis of cone penetration in soft clay. Comput Geotech 2009;36:851–60.
[15] Tolooiyan A, Gavin K. Modelling the cone penetration test in sand using cavity expansion and Arbitrary Lagrangian Eulerian finite element methods. Comput Geotech 2011;38:482–90.
[16] Qiu G, Henke S, Grabe J. Application of a Coupled Eulerian–Lagrangian approach on geomechanical problems involving large deformations. Comput Geotech 2011;38:30–9.
[17] Pucker T, Grabe J. Numerical simulation of the installation process of full displacement piles. Comput Geotech 2012;45:93–106.
[18] Jassim I, Hamad F, Vermeer P. Dynamic material point method with applications in geomechanics. In: 2nd Int Symp Comput Geomech (COMGEO II).
[19] Phuong NTV, van Tol AF, Elkadi ASK, Rohe A. Modelling of pile installation using the material point method (MPM). In: 8th Eur Conf Numer Methods Geotech Eng. p. 271–6.
[20] Engin HK. Modelling pile installation effects – a numerical approach. Delft University of Technology; 2013.
[21] Engin HK, Brinkgreve RBJ, van Tol AF. Simplified numerical modelling of pile penetration – the press-replace technique. Int J Numer Anal Methods Geomech 2015 [in press].
[22] Harlow FH. The particle-in-cell computing method for fluid dynamics. Methods Comput Phys 1964;3:319–43.
[23] Brackbill JU, Kothe DB, Ruppel HM. Flip: a low-dissipation, particle-in-cell method for fluid flow. Comput Phys Commun 1988;48:25–38.
[24] Sulsky D, Chen Z, Schreyer HL. A particle method for history-dependent materials. Comput Methods Appl Mech Eng 1994;118:179–96.
[25] Sulsky D, Schreyer HL. Axisymmetric form of the material point method with applications to upsetting and Taylor impact problems. Comput Methods Appl Mech Eng 1996;139:409–29.
[26] Bardenhagen SG, Brackbill JU. Dynamic stress bridging in granular material. J Appl Phys 1998;83:5732–40.
[27] Więckowski Z, Youn SK, Yeon JH. A particle-in-cell solution to the silo discharging problem. Int J Numer Methods Eng 1999;45:1203–25.
[28] Sulsky D. A numerical study of compaction of dry granular material. Mater Res Soc Symp, vol. 759. Cambridge University Press; 2002. p. MM3-1.
[29] Bardenhagen SG, Kober EM. The generalized interpolation material point method. Comput Model Eng Sci 2004;5:477–96.
[30] Więckowski Z. The material point method in large strain engineering problems. Comput Methods Appl Mech Eng 2004;193:4417–38.
[31] Coetzee CJ, Vermeer PA, Basson AH. The modelling of anchors using the material point method. Int J Numer Anal Methods Geomech 2005;29:879–95.
[32] Beuth L, Benz T, Vermeer PA, Wieckowski Z. Large deformation analysis using a quasi-static material point method. J Theor Appl Mech 2008;38:45–60.
[33] Jassim I, Stolle D, Vermeer P. Two-phase dynamic analysis by material point method. Int J Numer Anal Methods Geomech 2013;37:2502–22.
[34] Dong Y, Ma J, Wang D, Randolph MF. Assessment of applicability of the material point method in offshore geotechnical engineering. Anal Methods Pet Upstream Appl 2015:117.
[35] Dong Y, Wang D, Randolph MF. A GPU parallel computing strategy for the material point method. Comput Geotech 2015;66:31–8.
[36] Andersen KH, Andresen L, Jostad HP, Clukey EC. Effect of skirt-tip geometry on set-up outside suction anchors in soft clay. In: 23rd Int Conf Offshore Mech Arct Eng, vol. 1. Parts A B, ASME; 2004. p. 1035–44.
[37] Anaraki KE. Hypoplasticity investigated: parameter determination and numerical simulation. Delft University of Technology; 2008.
[38] Von Wolffersdorff PA. A hypoplastic relation for granular materials with a predefined limit state surface. Mech Cohesive-Frictional Mater 1996;1:251–71.
[39] Niemunis A, Herle I. Hypoplastic model for cohesionless soils with elastic strain range. Mech Cohesive-frictional Mater 1997;2:279–99.
[40] Masin D. Plaxis implementation of hypoplasticity; 2010.
[41] Phuong NTV, van Tol AF, Elkadi ASK, Rohe A. Numerical investigation of pile installation effects in sand using material point method. Comput Geotech 2016;73:58–71.
[42] Brinkgreve RBJ, Engin E, Swolfs WM. PLAXIS 2D; 2012.

Please cite this article in press as: Tehrani FS et al. Comparison of Press-Replace Method and Material Point Method for analysis of jacked piles. Comput Geotech (2016), http://dx.doi.org/10.1016/j.compgeo.2016.04.017